LETTERS

Demonstration of a spaser-based nanolaser

M. A. Noginov[1], G. Zhu[1], A. M. Belgrave[1], R. Bakker[2], V. M. Shalaev[2], E. E. Narimanov[2], S. Stout[1,3], E. Herz[3], T. Suteewong[3] & U. Wiesner[3]

One of the most rapidly growing areas of physics and nanotechnology focuses on plasmonic effects on the nanometre scale, with possible applications ranging from sensing and biomedicine to imaging and information technology[1,2]. However, the full development of nanoplasmonics is hindered by the lack of devices that can generate coherent plasmonic fields. It has been proposed[3] that in the same way as a laser generates stimulated emission of coherent photons, a 'spaser' could generate stimulated emission of surface plasmons (oscillations of free electrons in metallic nanostructures) in resonating metallic nanostructures adjacent to a gain medium. But attempts to realize a spaser face the challenge of absorption loss in metal, which is particularly strong at optical frequencies. The suggestion[4–6] to compensate loss by optical gain in localized and propagating surface plasmons has been implemented recently[7–10] and even allowed the amplification of propagating surface plasmons in open paths[11]. Still, these experiments and the reported enhancement of the stimulated emission of dye molecules in the presence of metallic nanoparticles[12–14] lack the feedback mechanism present in a spaser. Here we show that 44-nm-diameter nanoparticles with a gold core and dye-doped silica shell allow us to completely overcome the loss of localized surface plasmons by gain and realize a spaser. And in accord with the notion that only surface plasmon resonances are capable of squeezing optical frequency oscillations into a nanoscopic cavity to enable a true nanolaser[15–18], we show that outcoupling of surface plasmon oscillations to photonic modes at a wavelength of 531 nm makes our system the smallest nanolaser reported to date—and to our knowledge the first operating at visible wavelengths. We anticipate that now it has been realized experimentally, the spaser will advance our fundamental understanding of nanoplasmonics and the development of practical applications.

A spaser should have a medium with optical gain in close vicinity to a metallic nanostructure that supports surface plasmon oscillations[3]. To realize such a structure, we employed a modified synthesis technique for high-brightness luminescent core–shell silica nanoparticles[19,20]

known as Cornell dots. As illustrated in Fig. 1a, the produced nanoparticles are composed of a gold core, providing for plasmon modes, surrounded by a silica shell containing the organic dye Oregon Green 488 (OG-488), providing for gain.

Transmission and scanning electron microscopy measurements give the diameter of the Au core and the thickness of the silica shell as ~14 nm and ~15 nm, respectively (Fig. 1b, c). The number of dye molecules per nanoparticle was estimated to be 2.7×10^3, and the nanoparticle concentration in a water suspension was equal to 3×10^{11} cm^{-3} (Methods). A calculation of the spaser mode of this system (Fig. 1d) yields a stimulated emission wavelength of 525 nm and a quality (Q)-factor of 14.8 (Methods). We note that in gold nanoparticles as small as the ones used here, the Q-factor is dominated by absorption. But as we show below, the gain in our system is high enough to compensate the loss.

The extinction spectrum of a suspension of nanoparticles shown in Fig. 2 is dominated by the surface plasmon resonance band at ~520 nm wavelength and the broad short-wavelength band corresponding to interstate transitions between d states and hybridized s–p states of Au. The Q-factor of the surface plasmon resonance is estimated from the width of its spectral band as 13.2, in good agreement with the calculations. The spectra in Fig. 2 also illustrate that the surface plasmon band overlaps with both the emission and excitation bands of the dye molecules incorporated in the nanoparticles.

As illustrated in Fig. 3, the decay kinetics of the emission at 480 nm were non-exponential. Fitting the data with the sum of two exponentials resulted in two characteristic decay times, 1.6 ns and 4.1 ns. The absorption and emission spectra of OG-488 (Fig. 2) are nearly symmetrical to each other, as expected of dyes, and this allows us to assume that the peak emission cross-section, σ_{em}, is equal to the peak absorption cross-section, $\sigma_{abs} = 2.55 \times 10^{-16}$ cm^2, determined from the absorption spectrum of OG-488 in water at known dye concentration. With this value and using the known formula relating the strength and the width of the emission band with the radiative lifetime τ (see ref. 21 and Methods), we obtain an estimated radiative
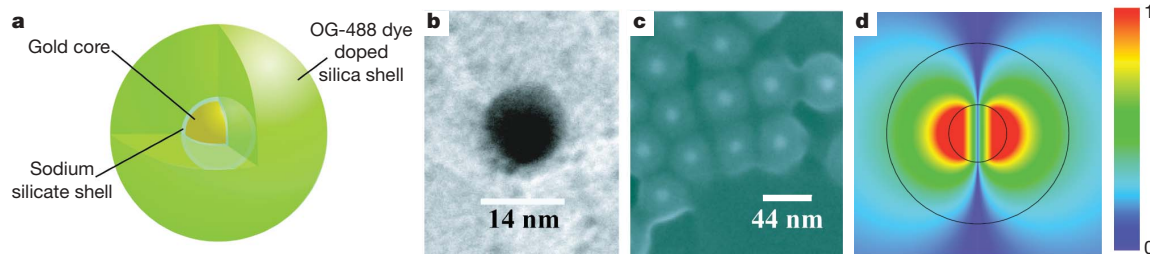

Figure 1 | Spaser design. a, Diagram of the hybrid nanoparticle architecture (not to scale), indicating dye molecules throughout the silica shell. **b,** Transmission electron microscope image of Au core. **c,** Scanning electron microscope image of Au/silica/dye core–shell nanoparticles. **d,** Spaser mode (in false colour), with $\lambda = 525$ nm and $Q = 14.8$; the inner and the outer circles represent the 14-nm core and the 44-nm shell, respectively. The field strength colour scheme is shown on the right.

[1]Center for Materials Research, Norfolk State University, Norfolk, Virginia 23504, USA. [2]School of Electrical & Computer Engineering and Birck Nanotechnology Center, Purdue University, West Lafayette, Indiana 47907, USA. [3]Materials Science and Engineering Department, Cornell University, Ithaca, New York 14850, USA.
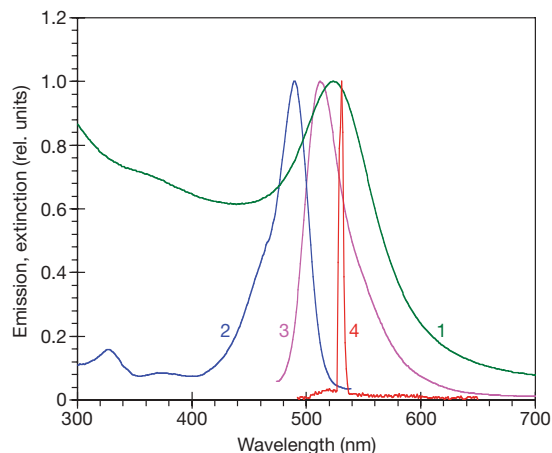
Figure 2 | Spectroscopic results. Normalized extinction (1), excitation (2), spontaneous emission (3), and stimulated emission (4) spectra of Au/silica/dye nanoparticles. The peak extinction cross-section of the nanoparticles is 1.1×10^{-12} cm^2. The emission and excitation spectra were measured in a spectrofluorometer at low fluence.

Figure 3 | Emission kinetics. Main panel, emission kinetics detected at 480 nm (1) and 520 nm (2). Inset, trace 1 plotted in semi-logarithmic coordinates (dots) and the corresponding fitting curve. The beginning of each emission kinetic trace coincides with the 90-ps pumping pulse.

lifetime of $\tau = 4.3$ ns that is very close to that of the slower component of the experimentally determined emission kinetics. We infer that the decay-time shortening (down to 1.6 ns) seen with the dye molecules in our effective plasmonic nanocavity can be explained by the Purcell effect[22].

When the emission was detected in the spectral band 520 ± 20 nm (which encompasses the maximum of the emission and gain), it first decayed and then developed a second peak (Fig. 3) that is characteristic of the development of a stimulated emission pulse[23] and consistent with the spaser effect (see below). In fact, both the delay of the stimulated emission pulse relative to the pumping pulse and the oscillating behaviour of the stimulated emission (relaxation oscillations) are known in lasers[23,24]; and because these phenomena do not depend on the nature of the oscillating mode, they are expected in spasers as well.

To study the stimulated emission, samples were loaded in cuvettes of 2 mm path length and pumped at wavelength $\lambda = 488$ nm with ~5-ns pulses from an optical parametric oscillator lightly focused into a ~2.4-mm spot. Whereas the emission spectra resembled those measured in the spectrofluorometer (Fig. 2) at weak pumping, a narrow peak appeared at $\lambda = 531$ nm (Fig. 4a) once the pumping energy exceeded a critical threshold value. Figure 4b gives the intensity of this peak as a function of pumping energy, yielding an input–output
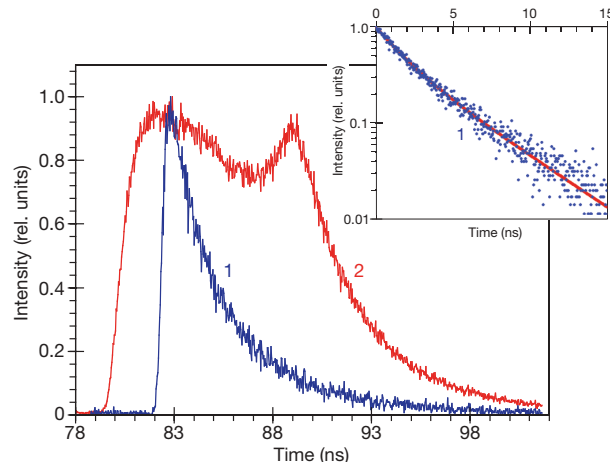
curve with a pronounced threshold characteristic of lasers. The ratio of the intensity of this laser peak to the spontaneous emission background increased with increasing pumping energy (Fig. 4b inset). By analogy with lasers, the dramatic change of the emission spectrum above the threshold (from a broad band to a narrow line) suggests that the majority of excited molecules contributed to the stimulated emission mode. As expected, the laser-like emission occurred at a wavelength at which the dye absorption, as evidenced by the excitation spectrum, is practically absent while the emission and the surface plasmon resonance are strong (see Fig. 2).

Diluting the sample more than 100-fold decreased the emission intensity, but did not change the character of the spectral line (Fig. 4a inset) or diminish the ratio of stimulated emission intensity to spontaneous emission background. We conclude from this that the observed stimulated emission was produced by single nanoparticles, rather than being a collective stimulated emission effect in a volume of gain medium with the feedback supported by the cuvette walls.

The spontaneous emission intensity of a 0.235 mM aqueous solution of OG-488 dye was approximately 1,000 times stronger than that of the lasing nanoparticle sample. But under pumping, the dye solution did not show spectral narrowing or superlinear dependence of the emission intensity on pumping power. The dependence of the emission intensity on pumping power was in fact sublinear, which could be a result of dye photo-bleaching. This control result is further
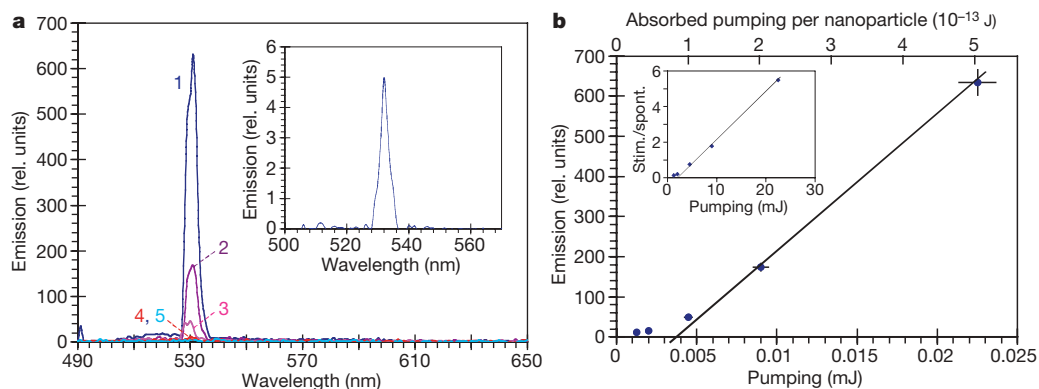

Figure 4 | Stimulated emission. a, Main panel, stimulated emission spectra of the nanoparticle sample pumped with 22.5 mJ (1), 9 mJ (2), 4.5 mJ (3), 2 mJ (4) and 1.25 mJ (5) 5-ns optical parametric oscillator pulses at $\lambda = 488$ nm. **b**, Main panel, corresponding input–output curve (lower axis, total launched pumping energy; upper axis, absorbed pumping energy per nanoparticle); for most experimental points, ~5% error bars (determined

by the noise of the photodetector and the instability of the pumping laser) do not exceed the size of the symbol. Inset of **a**, stimulated emission spectrum at more than 100-fold dilution of the sample. Inset of **b**, the ratio of the stimulated emission intensity (integrated between 526 nm and 537 nm) to the spontaneous emission background (integrated at <526 nm and >537 nm).

evidence that the stimulated emission occurs in individual hybrid Au/silica/dye nanoparticles, rather than in the macroscopic volume of the cuvette.

The diameter of the nanoparticle (hybrid Cornell dot) is 44 nm—too small to support visible stimulated emission in a purely photonic mode. But modelling of the system predicts that stimulated emission can occur in a much smaller surface plasmon mode if the number of excited dye molecules per nanoparticle exceeds 2.0×10^3 (Methods); this number is smaller than the number of OG-488 molecules available per nanoparticle in the experimental sample, which is $\sim 2.7 \times 10^3$. The pumping photon flux in our measurements ($\sim 10^{25}\, cm^{-2}\, s^{-1}$) exceeds the saturation level for OG-488 dye molecules ($\sim 10^{24}\, cm^{-2}\, s^{-1}$), so almost all the dye molecules were excited. The gain in the system was thus sufficiently large to overcome the overall loss, enabling the first experimental demonstration of a spaser, which we report here and regard as the central finding of the present work. But another important result is that the outcoupling of surface plasmon oscillations to photonic modes (facilitated by the radiative damping of the localized surface plasmon mode) constitutes a nanolaser that is realized by each individual nanoparticle, making it the smallest reported in the literature and the only one to date operating in the visible range.

The demonstrated phenomenon, involving resonant energy transfer from excited molecules to surface plasmon oscillations and stimulated emission of surface plasmons in a luminous mode, is consistent with the original theoretical proposal of a spaser[3] and the more recent concept of a 'lasing spaser'[25], which share many common features despite their differences in detail. We note that this phenomenon is very different from that exploited in quantum cascade lasers[26], in which the surface plasmon mode (almost indistinguishable at the mid-infrared wavelength and the geometry of the experiment from the photonic transverse electromagnetic mode) is used as a guiding mode in an otherwise normal laser cavity. In contrast, in the reported spaser, the oscillating surface plasmon mode provides for feedback needed for stimulated emission of localized surface plasmons. The ability of the spaser to actively generate coherent surface plasmons could lead to new opportunities for the fabrication of photonic meta-materials, and have an impact on technological developments seeking to exploit optical and plasmonic effects on the nanometre scale.

METHODS SUMMARY

The Methods section presents a detailed discussion of the following experimental and theoretical studies: (1) synthesis and cleaning of hybrid Au/silica/dye nanoparticles, (2) theoretical modelling of the spaser effect in hybrid core–shell nanoparticles, (3) emission kinetics measurements, and (4) calculation of the radiative decay lifetime from the emission spectra.

Full Methods and any associated references are available in the online version of the paper at www.nature.com/nature.

1.   Maier, S. A. *Plasmonics: Fundamentals and Applications* (Springer, 2007).
2.   Brongersma, M. L. & Kik, P. G. (eds), *Surface Plasmon Nanophotonics* (Springer Series in Optical Sciences, Vol. 131, Springer, 2007).
3.   Bergman, D. J. & Stockman, M. I. Surface plasmon amplification by stimulated emission of radiation: quantum generation of coherent surface plasmons in nanosystems. *Phys. Rev. Lett.* **90**, 027402 (2003).
4.   Sudarkin, A. N. & Demkovich, P. A. Excitation of surface electromagnetic waves on the boundary of a metal with an amplifying medium. *Sov. Phys. Tech. Phys.* **34**, 764–766 (1989).
5.   Nezhad, M. P., Tetz, K. & Fainman, Y. Gain assisted propagation of surface plasmon on planar metallic waveguides. *Opt. Express* **12**, 4072–4079 (2004).
6.   Lawandy, N. M. Localized surface plasmon singularities in amplifying media. *Appl. Phys. Lett.* **85**, 5040–5042 (2004).
7.   Noginov, M. A. *et al.* Enhancement of surface plasmons in an Ag aggregate by optical gain in a dielectric medium. *Opt. Lett.* **31**, 3022–3024 (2006).
8.   Noginov, M. A. *et al.* The effect of gain and absorption on surface plasmons in metal nanoparticles. *Appl. Phys. B* **86**, 455–460 (2007).
9.   Seidel, J., Grafstroem, S. & Eng, L. Stimulated emission of surface plasmons at the interface between a silver film and an optically pumped dye solution. *Phys. Rev. Lett.* **94**, 177401 (2005).
10. Noginov, M. A. *et al.* Compensation of loss in propagating surface plasmon polariton by gain in adjacent dielectric medium. *Opt. Express* **16**, 1385–1392 (2008).
11. Noginov, M. A. *et al.* Stimulated emission of surface plasmon polaritons. *Phys. Rev. Lett.* **101**, 226806 (2008).
12. Dice, G. D., Mujumdar, S. & Elezzabi, A. Y. Plasmonically enhanced diffusive and subdiffusive metal nanoparticle-dye random laser. *Appl. Phys. Lett.* **86**, 131105 (2005).
13. Popov, O., Zilbershtein, A. & Davidov, D. Random lasing from dye-gold nanoparticles in polymer films: enhanced gain at the surface-plasmon-resonance wavelength. *Appl. Phys. Lett.* **89**, 191116 (2006).
14. Kawasaki, M. & Mine, S. Novel lasing action in dye-doped polymer films coated on large pseudotabular Ag islands. *J. Phys. Chem. B* **110**, 15052–15054 (2006).
15. Muhlschlegel, P., Eisler, H.-J., Martin, O. J. F., Hecht, B. & Phol, D. W. Resonant optical antennas. *Science* **308**, 1607–1609 (2005).
16. Gordon, J. A. & Ziolkowski, R. W. The design and simulated performance of a coated nanoparticle laser. *Opt. Express* **15**, 2622–2653 (2007).
17. Noda, S. Seeking the ultimate nanolaser. *Science* **314**, 260–261 (2006).
18. Hill, M. T. *et al.* Lasing in metallic-coated nanocavities. *Nature Photon.* **1**, 563–564 (2007).
19. Enüstün, B. V. & Turkevich, J. Coagulation of colloidal gold. *J. Am. Chem. Soc.* **85**, 3317–3328 (1963).
20. Ow, H. *et al.* Bright and stable core-shell fluorescent silica nanoparticles. *Nano Lett.* **5**, 113–117 (2005).
21. Noginov, M. A. *et al.* Crystal growth and characterization of a new laser material, $Nd:Ba_5(PO_4)_3Cl$. *J. Opt. Soc. Am. B* **17**, 1329–1334 (2000).
22. Purcell, E. M. Spontaneous emission probabilities at radio frequencies. *Phys. Rev.* **69**, 681 (1946).
23. Noginov, M. A., Fowlkes, I., Zhu, G. & Novak, J. Neodymium random lasers operating in different pumping regimes. *J. Mod. Opt.* **51**, 2543–2553 (2004).
24. Svelto, O. *Principles of Lasers* 4th edn (Plenum, 1998).
25. Zheludev, N. I., Prosvirnin, S. L., Papasimakis, N. & Fedotov, V. A. Lasing spaser. *Nature Photon.* **2**, 351–354 (2008).
26. Sirtori, C. *et al.* Long-wavelength ($\lambda \approx 8$–11.5 μm) semiconductor lasers with waveguides based on surface plasmons. *Opt. Lett.* **23**, 1366–1368 (1998).

METHODS

Particle synthesis and cleaning. Gold cores with a thin sodium silicate shell were prepared according to previously published methods[19,27] and transferred into a basic ethanol (1 μl ammonium hydroxide per ml of ethanol) solution via dilution (1:4). Tetraethoxysilane was added (1 μl per 10 ml of Stöber synthesis solution) to grow a thick silica shell. Ten microlitres of OG-488 isothiocyanate or maleimide (Invitrogen, dissolved to 4.56 mM concentration in dimethylsulphoxide), were conjugated to 3-isocyanatopropyltriethoxysilane (ICPTS) or 3-mercaptopropyltrimethoxysilane (MPTMS), respectively in a 1:50 molar ratio (dye:ICPTS or dye:MPTMS) in an inert atmosphere and added to the aforementioned 10 ml of Stöber synthesis solution. The particles were cleaned by centrifugation and resuspended in water. The concentration of nanoparticles in the suspension, approximately $3 \times 10^{11}\,\mathrm{cm}^{-3}$, was calculated from the gold wt% measurements provided by Elemental Analysis, Inc. The number of dye molecules per particle, 2.7×10^3, was estimated on the basis of the known concentration of nanoparticles, the starting concentration of dye molecules used in the reaction, and the concentration of dye molecules which remained in the solution after the synthesis.

Theoretical model. To calculate the cold-cavity modes in the system, the structure is modelled as a spherical silica shell (refractive index of 1.46) with a gold core, whose frequency-dependent dielectric permittivity is taken from ref. 28 (Fig. 1a). The corresponding three-dimensional wave equation can be solved analytically using Debye potentials[29], which yields a sequence of localized plasmon modes with different values of total angular momentum ℓ and its projection m ($m = -\ell, ..., 0, ..., \ell$). The experimental wavelength range $\lambda \approx 530\,\mathrm{nm}$ corresponds to the lowest frequency modes of this sequence, $\ell = 1$, which are triply degenerate ($m = -1, 0, 1$). This degeneracy (similar to that in the p state of the hydrogen atom[30]) can be visualized in relation to a different direction of the mode 'axis' (Fig. 1d) and will be lifted by a deviation from spherical symmetry in the particle geometry. The resulting cold-cavity $\ell = 1$ mode wavelength (calculated with no fitting parameters) is 525 nm, and the Q-factor is 14.8 (where the primary contribution originates from the losses in the gold core).

For the active system, the gain is taken into account in the imaginary part of the refractive index of the silica shell, with the magnitude calculated using standard expressions of refs 24 and 29, and from the known value of the stimulated emission cross-section of OG-488 molecules and their density. In this approach, the lasing threshold relates to the zero of the imaginary part of the mode frequency (corresponding to infinite lifetime). Assuming that the active molecules are uniformly distributed from the core to the diameter of 24 nm (in the 44-nm-diameter silica shell), we find that the stimulated emission requires ~2,000 active molecules.

Emission kinetics measurements. Emission decay kinetics were measured using a fluorescence lifetime imaging microscope (Microtime 200). The samples were excited at $\lambda = 466\,\mathrm{nm}$ with <90 ps laser pulses at 40 MHz repetition rate. The emission was taken from the side of the pumping in an inverted microscope set-up (an immersion objective lens, a coverslip and a droplet of sample on the coverslip). The diameter and the depth of the focused laser beam were 0.24 μm and 1 μm, respectively, and the pumping power density was $9.8 \times 10^5\,\mathrm{W\,cm}^{-2}$ ($4.2 \times 10^4\,\mathrm{W\,cm}^{-2}$) when the emission was detected in the $480 \pm 5\,\mathrm{nm}$ ($520 \pm 20\,\mathrm{nm}$) spectral band. The response time of the detector was shorter than 300 ps. The fit of the emission kinetics detected at 480 nm with the sum of two exponents resulted in $I(t) \propto a_1 \exp(-t/\tau_1) + a_2 \exp(-t/\tau_2)$, with $a_1 = 0.48$, $a_2 = 0.52$, $\tau_1 = 1.6\,\mathrm{ns}$ and $\tau_2 = 4.1\,\mathrm{ns}$. Given the experimental noise, the characteristic decay times are determined with ±10% accuracy.

The observation of the stimulated emission kinetics (Fig. 2, trace 2) from such a tiny volume, which can provide for only very small amplification, is additional proof of the spaser and nanolaser effects occurring in individual nanoparticles.

Radiative lifetime. Evaluation of the radiative lifetime from the emission spectra was performed using the known formula

$$\sigma_{\mathrm{em}}(\lambda) = \frac{\lambda^5 I(\lambda)}{8\pi n^2 c \tau \int \lambda I(\lambda)\,\mathrm{d}\lambda}$$

where λ is the wavelength, $I(\lambda)$ is the emission intensity, n is the index of refraction, and c is the speed of light.

27. Mulvaney, P., Liz-Marzan, L. M., Giersig, M. & Ung, T. Silica encapsulation of quantum dots and metal clusters. *J. Mater. Chem.* **10**, 1259–1270 (2000).
28. Johnson, P. B. & Christy, R. W. Optical constants of the noble metals. *Phys. Rev. B* **6**, 4370–4379 (1972).
29. Born, M. & Wolf, E. *Principles of Optics* 6th edn (Cambridge Univ. Press, 1998).
30. Landau, L. D. & Lifshits, E. M. *Quantum Mechanics: Non-Relativistic Theory* (Pergamon, 1977).